X-ray diffuse-scattering study of the pinned charge-density waves in tetramethyltetraselenafulvalene dimethyltetracyanoquinodimethane (TMTSF-DMTCNQ) disordered by irradiation

L. Forro and L. Zuppiroli
Section d'Etude des Solides Irradiés, Centre d'Etudes Nucléaires de Fontenay-aux-Roses, 92260 Fontenay-aux-Roses, France

J. P. Pouget and K. Bechgaard*
Laboratoire de Physique des Solides, Université de Paris-Sud, 91405 Orsay, France
(Received 12 July 1982)

We present an x-ray diffuse-scattering study of the quasi-one-dimensional conductor tetramethyltetraselenafulvalene dimethyltetracyanoquinodimethane (TMTSF-DMTCNQ) containing different amounts of irradiation-induced disorder. The pinning of the charge-density waves (CDW) to the defects destroys the three-dimensional long-range order even at 10 K, and anisotropically broadened reflections appear in the irradiated samples instead of the superstructure reflections in the pure sample. The values of the longitudinal as well as transverse correlation lengths have been measured as a function of the temperature and the irradiation dose. They have been interpreted within the framework of a model where each defect pins the charge-density wave in a given volume of the crystal. This volume should contain three chain segments of ten molecules. At small defect concentrations, the intensity of the thermal $4k_F$ anomaly observed in the pure TMTSF-DMTCNQ decreases and becomes almost undetectable at 0.3 mol % defect concentration. At higher doses, of 0.7 and 2.8 mol %, the $4k_F$ anomaly is resurrected by the defects and becomes static in the whole temperature range. Strong similarities in the temperature behavior of $2k_F$ and $4k_F$ scatterings in the TMTSF salt containing 1 or 2 mol % of radiation defects and in other unirradiated organic conductors such as Qn(TCNQ)$_2$ (quinolinium tetracyanoquinodimethane), have been observed.

I. INTRODUCTION

The role of structural disorder in low-dimensional systems with charge-density-wave instabilities of the electron gas is a subject of recent interest. The pinning of charge density waves (CDW) to defects was shown to be essential for the understanding of the electronic properties of quasi-one-dimensional trichalcogenides, such as niobium triselenide[1] ($NbSe_3$), of dichalcogenides such as tantalum disulfide[2] (TaS_2), and of organic conductors such as tetrathiafulvalene tetracyanoquinodimethane[3] (TTF-TCNQ).

Irradiation has been used several times to produce disorder in a controlled way in charge-density-wave systems.[4,5] It is demonstrated that it creates strong pinning centers in low concentrations, the order of magnitude of which can be estimated easily,[6] especially in organic conductors where the defect content can be determined experimentally and rather accurately.[7] Tetramethyltetraselenafulvalene dimethyltetracyanoquinomethane (TMTSF-DMTCNQ) is one of the most interesting organic conductors which exhibits a clear charge-density-wave-driven metal-insulator phase transition.[8,9] Below 42 K and at ambient pressure it is a Peierls insulator. But under a pressure of 10 kbar, the high-temperature metallic state is stabilized down to 1.2 K.[10] In the best samples investigated recently,[11] the resistivity ratio under pressure $\rho_{300\,K}/\rho_{4.2\,K}$ is larger than 100. TMTSF-DMTCNQ is also one of the organic conductors in which the effects of disorder have been most extensively studied. It has been demonstrated that irradiation-induced defects, present with a concentration of 0.2 mol %, increase the conductivity of the Peierls insulator by 3 orders of magnitude at 4.2 K.[12,13] Hall-effect and thermopower measurements have shown that this change is due to a strong increase in the number of carriers. A weak irradiation-induced disorder destroys the Peierls insulating state and extends the metallic state below 42 K.[13] It was conjectured that this stabilization of the metallic state is due to the loss of spatial periodicity of charge-density waves in the presence

of the strong pinning centers[5]: each irradiation-induced defect pins the charge-density waves in a given volume of the sample, the high foreign potential defining rigidly the phase of a piece of charge-density waves. The low-temperature transport properties of irradiated samples were analyzed phenomenologically either as the consequence of a random distribution of conducting volumes created in an insulating Peierls matrix[14] or as the consequence of a discommensuration network where new carriers were created at phase defects of the charge-density waves. But these intuitions were suggested mainly from transport experiments. A more direct investigation is necessary to check the spatial distribution of charge-density waves in the presence of disorder. This is one of the reasons for the present x-ray diffuse-scattering study of irradiated TMTSF-DMTCNQ.

X-ray diffuse scattering is known to be one of the most important tools for the study of structural instabilities of quasi-one-dimensional conductors related to the presence of charge-density waves. TMTSF-DMTCNQ is one of the best candidates for the application of this experimental method. The study of the pure sample was previously reported in Ref. 9 and completed recently in Refs. 15 and 16. The x-ray pattern shown in Fig. 1 clearly exhibits $2k_F$ diffuse sheets due to the x-ray scattering by quasi-one-dimensional lattice fluctuations, which are visible from 42 to 225 K in the pure samples. The observed sheets correspond mostly to a modulation of the TMTSF stacks.[16] Furthermore, the $2k_F$ scattering is commensurate, $2k_F=a^*/4$, and presents modulations well above the Peierls transition, indicating substantial lateral correlations between charge-density waves up to at least 175 K.[9] At the phase transition, the $2k_F$ diffuse sheets condense into well-defined satellite Bragg reflections, of reduced wave vector $\vec{q}(\frac{1}{4},\frac{1}{3},0)$, due to a long-range ordering of the charge-density waves. In the present paper the effects of structural disorder on the $2k_F$ diffuse sheets and satellite reflections are studied. The temperature dependence of the longitudinal as well as the transverse correlation lengths of the charge-density-wave packets in the presence of strong pinning centers have also been measured as a function of the concentration of defects.

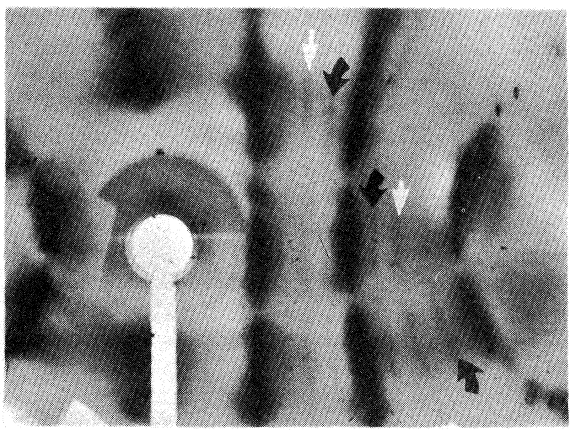

FIG. 1. X-ray pattern of pure TMTSF-DMTCNQ at 125 K showing the $2k_F$ (black arrows) and $4k_F$ (white arrows) diffuse lines, at $0.25a^*$ and $0.50a^*$ reduced-zone wave vectors, respectively, coming from the intersection of the Edwald sphere with diffuse sheets at the corresponding wave vector. In this pattern the a chain direction is horizontal and the reciprocal space shown is close to the (a^*,b^*) plane. (This pattern, from Ref. 15, is free from $\lambda/2$ contamination.)

An unexpected instability, discovered with x-ray diffuse-scattering experiments in several one-dimensional organic conductors, is the instability which is occurring at the $4k_F$ wave vector. It has been observed at and below room temperature in pure TMTSF-DMTCNQ (Fig. 1), but unlike the $2k_F$ anomaly, it always keeps the aspect of diffuse sheets, and does not condense into satellite reflections at low temperatures. A study of its temperature dependence reveals its dynamical origin (phonon anomaly).[15] An analysis of its structure factor shows that it corresponds, as the $2k_F$ anomaly, to fluctuations located mainly on the TMTSF chain.[15] The crude interpretation of the $4k_F$ anomaly in terms of "spinless fermions" localized in a Wigner lattice,[17] as well as the more subtle calculation of Emery,[18] attribute it to lattice effects induced by substantial electron Coulomb interactions. In the present paper the introduction of irradiation disorder in TMTSF-DMTCNQ is shown to modify the $4k_F$ scattering in an unexpected and interesting way.

It is worth mentioning briefly at the end of this Introduction that two more qualitative investigations of charge-density waves in the presence of irradiation-induced disorder have been published previously.[19] They were performed on the two inorganic solids: the quasi-one-dimensional tantalum trisulfide TaS_3 and the layered tantalum disulfide TaS_2, and electron microdiffraction was used instead of x-ray scattering.

II. EXPERIMENTAL CONDITIONS

The present study was carried out with the fixed-film, fixed-crystal method. The experimental setup is identical to that used in previous studies of one-dimensional conductors.[20] Films were placed on a large-size beryllium window of a cylindrical low-temperature camera. The temperature was lowered using a cryocooler and regulated within a few tenths

of a degree between 10 and 300 K. From the x-ray source, the Cu$K\alpha$ radiation (1.54 Å) was selected after reflection on a doubly bent pyrolytic graphite monochromator. However, the use of the (002) reflection leads to a $\lambda/2$ contamination of x-ray patterns from the continuous spectrum of the x-ray source.

Earlier studies[20] have shown that the widths of superlattice reflections or of diffuse lines are directly proportional to the correlation lengths of charge-density waves. They can be measured by reading the x-ray patterns with a microdensitometer. The inverse correlation length in a given direction has been obtained from these readings by subtraction of the experimental resolution from the measured half-width at half maximum (HWHM) of the diffuse scattering (Lorentzian resolution correction). The experimental resolution has been obtained from the HWHM of sharp reflections (additional and weak Bragg reflections arising from the $\lambda/2$ contamination) at about the same scattering angle. It was found to be 0.036 $Å^{-1}$ along a^* and 0.06 $Å^{-1}$ along b^* (throughout this study one uses the convention $\vec{a}\cdot\vec{a}^* = 2\pi$).

X rays are well known to be able to damage organic conductors.[7] Earlier studies of TMTSF-DMTCNQ (Ref. 16) have shown that crystals irradiated during x-ray diffuse scattering in the Orsay device are damaged at a rate of the order of 0.02 mol % molecular defect fraction per day of exposure. For each sample investigated here, the total exposure to x rays did not exceed one day. Thus, except for the sample with 0.1% defect concentration, the damage produced during the experiment could be neglected. This is also the reason for producing the defects in a much more powerful x-ray beam, in direct contact with the primary beam of a Cu$K\alpha$ x-ray tube.

The defect concentration was determined from dc transport properties at room temperature by simul-

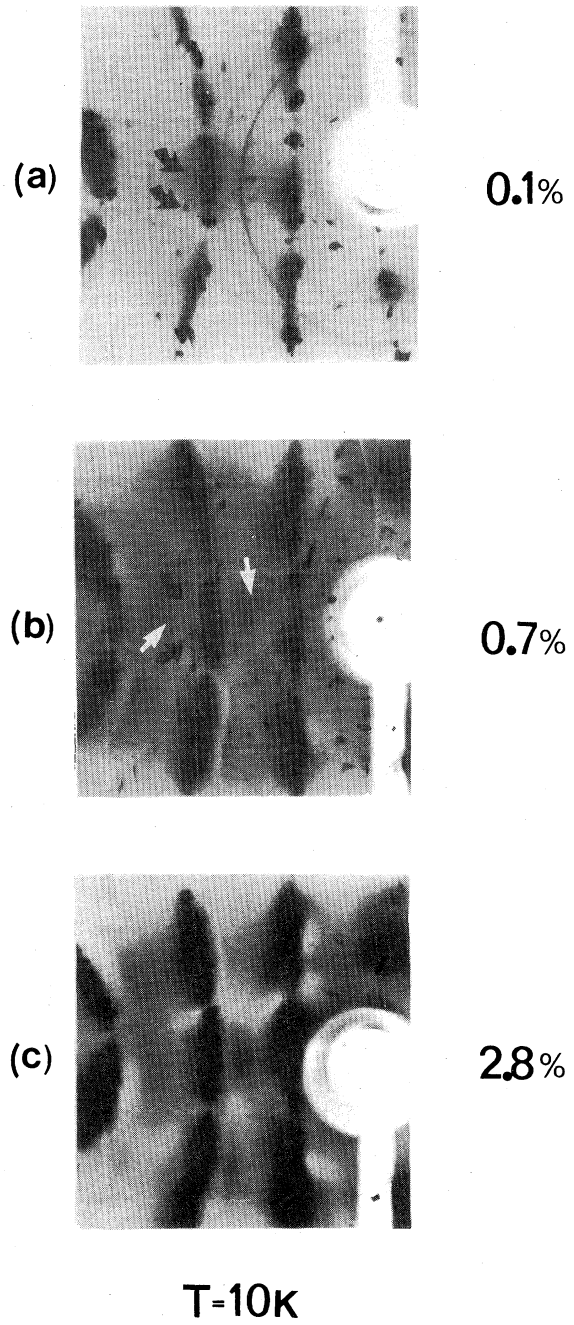

FIG. 2. X-ray patterns of TMTSF-DMTCNQ at 10 K, for various defect concentrations. They have been taken nearly in the same orientation as in Fig. 1. (a) 0.1 mol % of defects; black arrows point to the $2k_F$ scattering condensed into well-defined satellite reflections at $\vec{q}=(\frac{1}{4},\frac{1}{3},0)$ reduced wave vector. No $4k_F$ scattering can be detected (additional Bragg spots in layers $h=0.5a^*$ and $1.5a^*$ are due to $\lambda/2$ contamination and rings observed around the incident beam is diffraction coming from the sample holder). (b) 0.7 mol % of defects: black arrows point to the previous satellite reflections noticeably broadened along b^*. Weak diffuse lines are also present at the $4k_F$ wave vector (white arrows). (c) 2.8 mol % of defects: only $2k_F$ lines are clearly visible (the modulation of their intensity in line direction comes mostly from x-ray interferences between Se atoms of the TMTSF molecule). These $2k_F$ lines are asymetrically broadened along a^* toward the position of the $4k_F$ anomaly which is now undetectable by eye. It is worth mentioning at such a low temperature, the large increase of the diffuse intensity surrounding main Bragg reflections when one passes from x-ray patterns (a) to (c). This reflects, via the x-ray scattering, the increasing amount of disorder on the average lattice, induced by the increasing number of defects created by irradiation.

taneous measurements of longitudinal and transverse resistivities. The defects detected by this method described in Ref. 6 are those which produce random potentials high enough to interrupt the conducting chains and change them in an assembly of metallic segments. Recent EPR experiments performed on irradiated TMTSF-DMTCNQ (Ref. 21) have demonstrated that the number of spins localized by the defects are indeed of the same order as the number of potentials counted at high temperatures. They have also confirmed the picture of magnetic segments bounded by the defects. The precise chemical and crystallographical nature of the defects is not yet known, but in the case of TMTSF-DMTCNQ a recent speculation suggests that $\frac{1}{4}$ of irradiation defects are induced on the TMTSF chains and $\frac{3}{4}$ on the DMTCNQ chains.[21] Finally, measurements of the volume change of irradiated samples have shown that each defect increases the volume of the crystal by about one molecular volume, suggesting that the defects involve large local molecular reorganizations.[22] In the present study we have investigated, between room temperature and 10 K, samples with 0.1-, 0.3-, 0.7-, and 2.8-mol % of radiation-induced defects.

III. RESULTS

The defects created by irradiation affect mostly the low-temperature behavior of the $2k_F$ instability. The main effects are summarized in the x-ray patterns of Fig. 2. These have been taken at the same temperature of 10 K and with different defect concentrations. At the low concentration of 0.1 mol % [Fig. 2(a)] sharp satellite reflections, associated with a three-dimensional (3D) ordering of the charge-density wave, are still present. But the transition temperature is lowered by 20 K with respect to the pure sample (this result is in agreement with the previous resistivity measurements.[13]) Increasing defect concentration gradually changes the diffuse spots in diffuse sheets. In the sample with 0.7 mol % [Fig. 2(b)] the superstructure modulation is still observed, but strongly broadened inside the $2k_F$ diffuse sheets. Any clear Peierls transition cannot be detected, but a short-range lateral order between $2k_F$ distortions of neighboring chains still remains. In the sample containing 2.8-mol % irradiation defects, the $2k_F$ charge-density waves are still detectable, but there is no modulation of the $2k_F$ intensity within the sheet, apart from the modulation coming from the molecular structure factor of the TMTSF molecule. There is no more short-range lateral order. In addition, the $2k_F$ diffuse sheets are strongly and asymmetrically broadened in the a^* direction. These points are further illustrated by microdensitometer scans of the $2k_F$ scattering at 10 K along the b^* and a^* directions shown in Figs. 3(a) and 3(b), respectively.

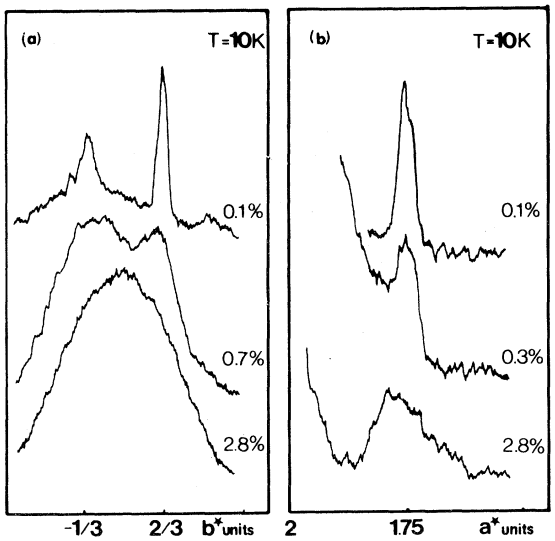

FIG. 3. Microdensitometer readings of x-ray patterns taken at 10 K for various defect concentrations: (a) scan in the b^* direction along the $h=2.25a^*$ diffuse line of Fig. 2. Satellite reflections (0.1-mol % defects) and short-range order (0.7-mol % defects) shown, correspond to arrows of Fig. 2. The smooth intensity variation within the last scan (2.8-mol % defects) is due to structure factor change in the reciprocal space. (b) Scan in the a^* direction across the $2k_F$ satellite spots (0.1-mol % defects), short-range order (0.3-mol % defects), and diffuse line (2.8-mol % defects). Note for the last scan, the asymmetrical broadening of the $2k_F$ diffuse sheet.

Figure 4 illustrates the effects of temperature on the $2k_F$ scattering. It concerns two samples containing 0.1- and 0.7-mol % defect mole fraction, respectively. It confirms that the effects of the defects on the $2k_F$ scattering are mainly visible at low temperatures. More quantitatively, Figs. 5 and 6 give the temperature dependence of the half-width at half maximum of the $2k_F$ scattering along the a^* and b^* directions, respectively. At low temperatures the deviations from the pure sample behavior increase with the amount of defects on both longitudinal and transverse linewidths.

Finally, one should notice that the second-order momentum (HWHM) given in Fig. 5 does not describe completely the shape of the $2k_F$ scattering along a^* in the two most irradiated samples. As shown clearly at 10 K in Fig. 4 for the 0.7-mol % sample, and in Figs. 2(c) and 3(b) for the samples with 2.8-mol % of defects, the line shape is very asymmetric and presents a long tail toward the larger wave-vector components in the a^* direction. Nevertheless, the intensity maximum of the line

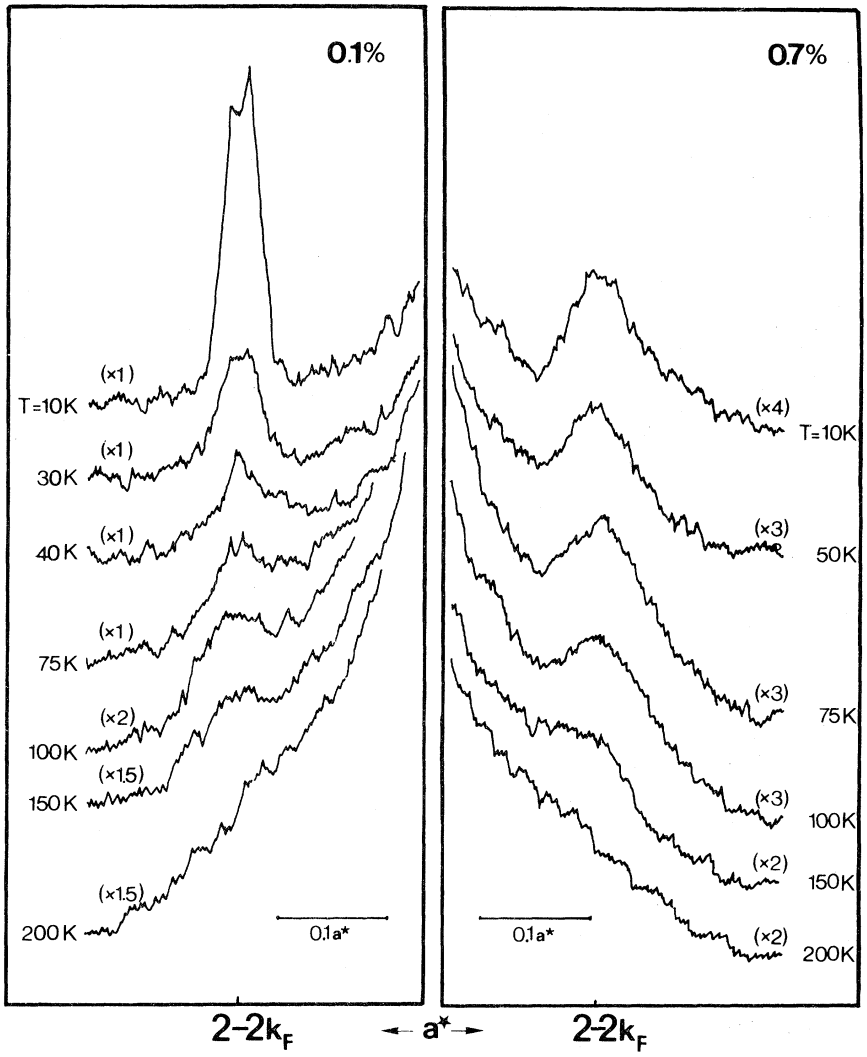

FIG. 4. Microdensitometer reading across the $2k_F$ lines in the a^* direction of x-ray patterns of samples with 0.1-mol % (a) and 0.7-mol % (b) defect concentration, for various temperatures. In the former case the $2k_F$ scattering condenses in satellite spots below 20 K, while in the latter it does not. Note also for both samples a very similar variation of $2k_F$ precursors in the high-temperature range. (The intensities for the two samples are not in scale.)

remains centered at the value $2k_F=0.25a^*$.

We now present the results concerning the $4k_F$ instability. Pure TMTSF-DMTCNQ shows above 60 K diffuse sheets of the $0.5a^*$ wave vector in chain direction (Fig. 1). With the increasing amount of defects, this scattering decreases in intensity and becomes observable on a more reduced temperature range. But it remains visible at room temperature on all samples investigated. The surprising behavior occurs at low temperature in the two most irradiated samples; the $4k_F$ scattering is resurrected by the defects and becomes observable down to 10 K. This has been clearly shown by x-ray patterns shown in Fig. 2. At 10 K there is no $4k_F$ scattering observable in the 0.1-mol % defects samples [Fig. 2(a)] as in pure TMTSF-DMTCNQ.[15] However, Fig. 2(b), taken with a sample containing 0.7 mol % of defects, shows a weak $4k_F$ scattering at 10 K. It appears more clearly on the microdensitometer reading shown in Fig. 7 for this sample.

Figure 8 summarizes the temperature ranges in which the $4k_F$ scattering is observed in the various samples studied and gives an estimate of the concentration dependence of its intensity. Clearly two concentration ranges have to be distinguished: At low defect concentration the intensity of the $4k_F$ scattering decreases with decreasing temperature and also decreases with increasing amount defects, while at

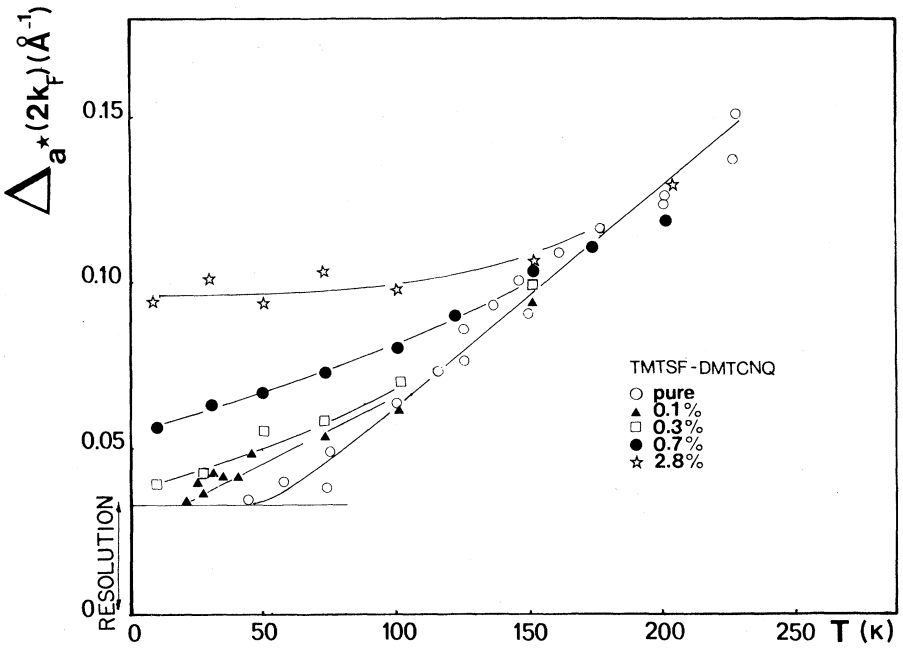

FIG. 5. Temperature dependence of the half-width at half maximum of the $2k_F$ scattering along the a^* direction $\Delta_{a^*}(2k_F)$, for samples with various defect concentrations (mol %). After subtraction of the experimental resolution, this quantity gives the inverse $2k_F$ correlation length in chain direction: $\xi_a^{-1}(2k_F)$ (data for the pure sample are from Ref. 15).

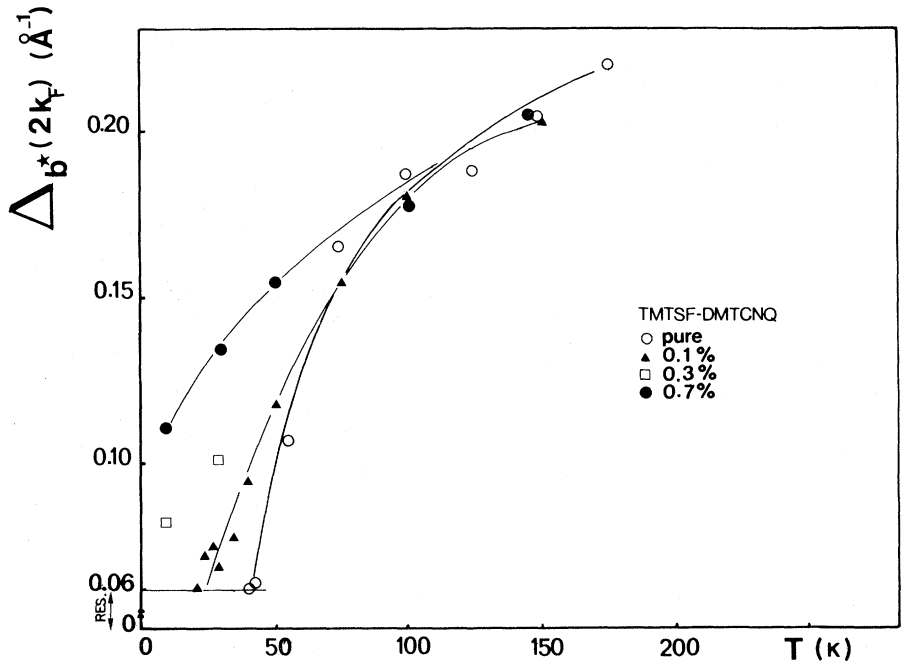

FIG. 6. Temperature dependence of the half-width at half maximum of the short-range order within the $2k_F$ scattering along the b^* direction $\Delta_{b^*}(2k_F)$, for samples with various defect concentrations (mol %). After subtraction of the experimental resolution, this quantity gives the inverse $2k_F$ correlation length in the transverse b direction: $\xi_b^{-1}(2k_F)$ (data for the pure sample are from Ref. 16). As the sample with 2.8 mol % of defects does not present a lateral modulation of its $2k_F$ scattering, no data corresponding to this concentration are shown in this figure.

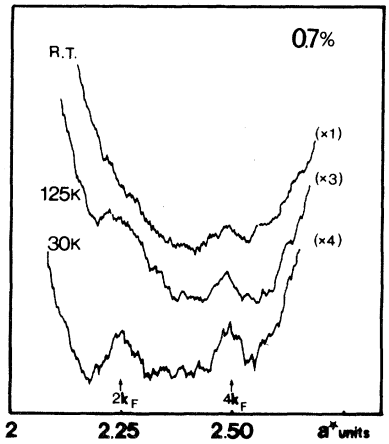

FIG. 7. Microdensitometer reading along a^* of x-ray patterns of the sample with 0.7-mol % defects, at different temperatures. Note the different temperature dependence of $2k_F$ and $4k_F$ scattering.

high defect concentration there is a resurrection of the intensity of the $4k_F$ scattering which becomes temperature independent. The temperature dependence of the $4k_F$ peak intensity is shown in Fig. 9 for the samples with 0.1- and 0.7-mol % defect concentrations.

It must be noticed (Fig. 7) that a temperature-independent $4k_F$ scattering can coexist with a temperature-dependent $2k_F$ scattering. Finally, Fig. 10 gives the half-width at half maximum along a^* of the $4k_F$ scattering. This quantity is, within experimental error, temperature independent, as in pure TMTSF-DMTCNQ.[15] Surprisingly, Fig. 10

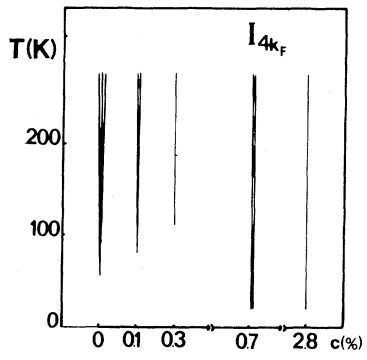

FIG. 8. Temperature range where the $4k_F$ scattering of TMTSF-DMTCNQ with different defect concentrations is observed. (The number of lines is roughly proportional to the $4k_F$ intensity). At lower concentrations ($c=0$, 0.1, and 0.3 mol %) the $4k_F$) intensity decreases with increasing defect concentration and with decreasing temperature. For $c=0.7$ and 2.8 mol % the $4k_F$ intensity is temperature independent. Note the increase of the $4k_F$ intensity when one passes from $c=0.3$ to 0.7 mol %.

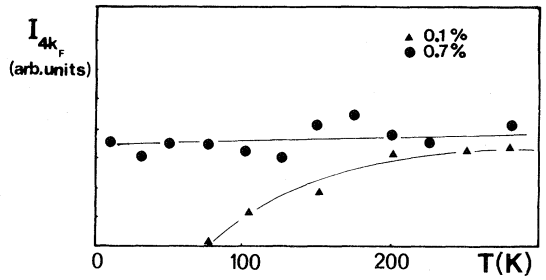

FIG. 9. Peak intensity of the $4k_F$ scattering as a function of temperature for various defect concentrations. Note the temperature-dependent intensity for the sample with 0.1-mol % defect concentration and temperature-independent behavior for the sample with 0.7-mol % defect concentration.

shows that the width of the $4k_F$ scattering does not change appreciably with the amount of defects and seems to be sensitive to the fact that the $4k_F$ scattering might be a temperature-independent (quasielastic) scattering.

IV. DISCUSSION

In pure TMTSF-DMTCNQ, $2k_F$ and $4k_F$ instabilities seem to demonstrate decoupled behaviors.[15] The $2k_F$ instability leads to the Peierls transition at 42 K, while the $4k_F$ instability disappears at low temperatures. Under irradiation and up to at least 2.8 mol % of defects, the $2k_F$ and $4k_F$ instabilities are still present and still decoupled. This is a reason for discussing the two anomalies separately.

A. The $2k_F$ scattering

One of the main results of the present study is the proof that charge-density waves are still present in samples containing defects strong enough to interrupt the conducting chains, in a concentration as large as 2.8 mol % (a strong pinning center every 30 molecules along the chains). At this concentration there is no phase transition anymore and the resistance versus temperature curve is simply activated on the whole temperature range.[23] The number of free carriers deduced from the Hall coefficent is of the order of 10^{20} cm^{-3} and is constant from 4.2 K to room temperature.[13] Thus the changes due to irradiation are more related to changes in the longitudinal and transverse coherences of the distortion than to the disappearance of the CDW's themselves. This kind of observation has also been done in other charge-density-wave systems such as monoclinic TaS_3 or 1T-TaS_2.[19] In some of these samples containing 10 mol % of strong pinning defects, a CDW superstructure is still observable at any temperature.

Let us discuss more quantitatively the longitudi-

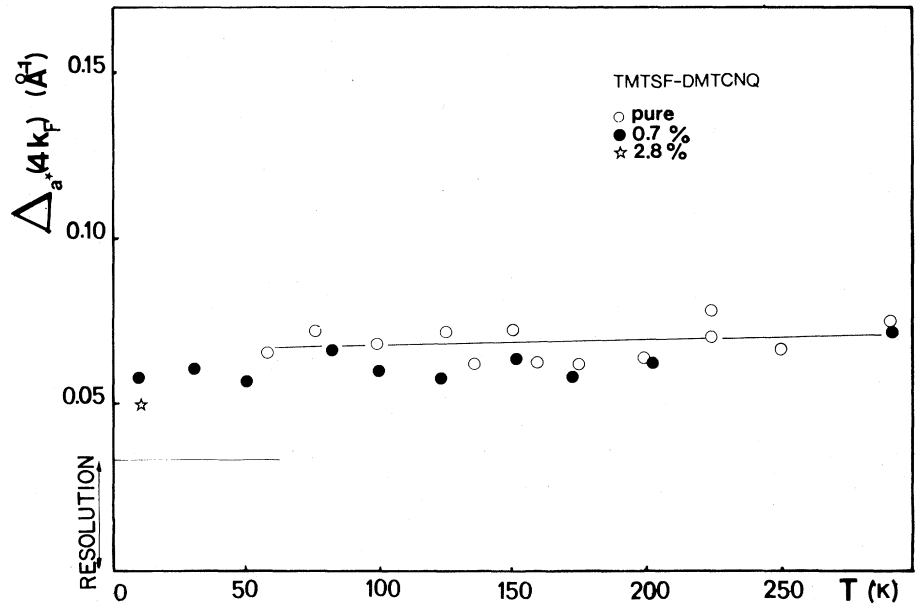

FIG. 10. Half-width at half maximum of the $4k_F$ scattering along the a^* direction $\Delta_{a^*}(4k_F)$, for samples with various defect concentrations (mol %). After subtraction of the experimental resolution, this quantity gives the inverse $4k_F$ correlation length in the chain direction: $\xi_a^{-1}(4k_F)$. Note that within experimental errors $\xi_a^{-1}(4k_F)$ is roughly independent of temperature and defect concentration (data for the pure sample are from Ref. 15).

nal ξ_a and transverse ξ_b correlation lengths deduced from Figs. 5 and 6 and calculated explicitly in Table I after correction of the experimental resolution. Above 150 K the values measured in all the samples, either pure or irradiated TMTSF-DMTCNQ, converge towards a common value. In that temperature range the charge-density-wave packet is very small ($\xi_a \lesssim 15$ Å and $\xi_b \lesssim 8$ Å) and the correlation lengths are limited mainly by phonons, as in the pure compound.

Strong deviations from the behavior of pure TMTSF-DMTCNQ occur below 150 K, at a temperature depending on the defect concentration. This means that in the low-temperature range, the defects play the most important role in the loss of coherence of charge-density waves. This direct observation of the loss of long-range order has been predicted from earlier transport studies of irradiated organic conductors.[12,13]

The following simple model is an attempt to account for the longitudinal and transverse variations of the coherence lengths with the defect concentration. Assuming that defects act as strong pinning centers, the configuration of the charge-density waves resembles the schematic picture of Fig. 11. Each defect pins the phase of the charge-density wave in a volume containing $n_a \times n_b \times n_c$ molecules. At low defect concentrations $[c < (n_a n_b n_c)^{-1}]$, the

TABLE I. Correlation lengths in angstroms along the a and b directions deduced from the half-width maximum of the $2k_F$ scattering (Figs. 7 and 8), after a Lorentzian resolution correction, for different defect concentrations and temperatures.

		c (mol %)			
T (K)		0.1	0.3	0.7	2.8
10 K	ξ_a (Å)	>200	150	50	15
	ξ_b (Å)	>200	50	20	
50 K	ξ_a (Å)	70	55	30	15
	ξ_b (Å)	16	16	10	
100 K	ξ_a (Å)	35	27	20	15
	ξ_b (Å)	8	8	8	

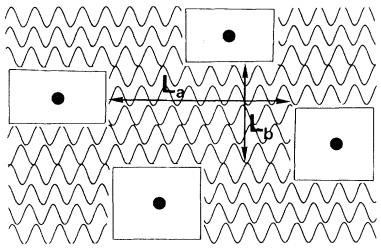

FIG. 11. Schematic representation of ordered charge-density waves in the presence of strong defects. L_a and L_b denote the dimension of the unperturbed volume which diffuses x rays coherently.

diffuse scattering is due mainly to the unperturbed part of the crystal. The satellite spots are broadened with respect to those of unirradiated crystals, because of the presence of pieces of pinned charge-density waves, which act as boundaries where the spatial coherence of the phase of the unperturbed CDW's is lost. In this simple picture of well-defined perturbed and nonperturbed volumes, the correlation length ξ, inverse of the HWHM of the scattering along a given reciprocal direction, is connected to the average size L, of the diffuse volume along the corresponding direction by the Scherrer formula[24]

$$L = 0.888\pi\xi.$$

Thus the prediction of the experimental correlation lengths reduces to a simple geometrical calculation of the parameters L_a, L_b, and L_c determining the average sizes of unperturbed zones along each direction. Along the direction a, for example, a given chain contains a number of perturbed segments corresponding, on average, to the concentration $c_a = n_b n_c c$, each perturbed segment containing n_a sites. The probability that an unperturbed segment of the chain contains n molecules can be written

$$p(n)\,dn = c_a\,dn \exp[-c_a(n+n_a)],$$

where $\exp[-c_a(n+n_a)]$ is the probability for the distance between two random defects to be greater than $n+n_a$ sites. Finally, the average distance L_a can be written

$$L_a = a\int_0^{+\infty} dn\, n_b n_c c n \exp\{-[n_b n_c c(n+n_a)]\}$$
$$= a(n_b n_c c)^{-1} \exp[-(n_a n_b n_c c)].$$

L_b and L_c are obtained by a circular permutation of the indices.

In the present geometrical model the ratio L_a/L_b is found to be defect-concentration independent. This is indeed in good agreement with the experimental values reported in Figs. 5 and 6 and in Table I. In Fig. 12 the experimental values ξ_a and ξ_b at 10 K have been plotted versus concentration. The present model fits these two curves quite satisfactorily, provided that the sizes of the perturbed volumes are $n_a = 10$, $n_b = 3$, and $n_c = 1$. At a concentration of 2.8 mol % the agreement between experiment and theory is, of course, poor. This is not surprising because then the product $n_a n_b n_c c$ is 84 mol %, demonstrating that a large fraction of the crystal is composed of perturbed volumes. The number of charge-density waves pinned around the defects is thus large enough to scatter the x rays appreciably. These are probably responsible for the asymmetric tails in the $2k_F$ diffuse lines observed at this concentration [Fig. 3(b)]. It could be attributed to local charge-transfer modulations due to the presence of charged defects. In order to screen the net charge of the defects, phase changes of the charge-density waves might occur in their vicinity. If defects are created mostly with the same charge, the charge compensation will occur always with the same sign leading to a given shift of the $2k_F$ wave vector. This point requires further investigation.

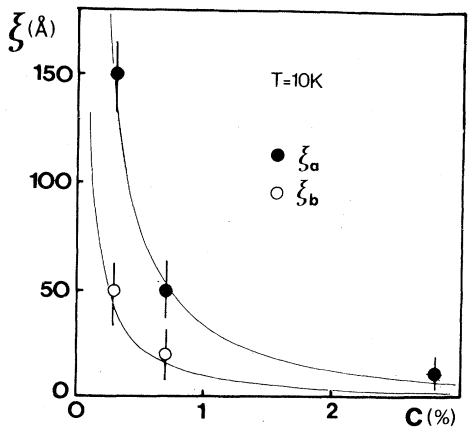

FIG. 12. Correlation lengths ξ_a, ξ_b measured at 10 K plotted vs defect concentration c (molecular fraction). The solid lines represent the fit by the model given in the discussion.

B. The $4k_F$ scattering

In pure TMTSF-DMTCNQ the $4k_F$ scattering is believed to have a dynamical origin (phonon anomaly) which does not increase as the temperature decreases. This statement is based on the fact that the width of the anomaly is temperature independent and that its intensity, corrected by the thermal population factor, remains constant.[15] Therefore, as the temperature decreases the intensity of the $4k_F$ scattering vanishes because of the decrease of the phonon population number. With few defects creat-

ed by irradiaton, the same behavior is observed. However, the phonon anomaly appears to be less pronounced. At room temperature its intensity decreases with the amount of defects in such a way that it becomes hardly visible. The temperature range where it can be observed decreases with an increasing amount of defects (Fig. 8). A qualitative explanation of the disappearance of the $4k_F$ anomaly at low temperatures and low-irradiation doses, without any observable broadening, could be obtained in the model of Emery,[18] where the modulation of the two-particle Coulomb interaction V_{ij} is responsible for the $4k_F$ scattering. In the low-concentration range, the strongly correlated charge-density waves, helped by a phonon modulation of V_{ij}, remain the source of the anomaly. With the pinning of charge-density waves around defects, the dynamical modulation of the Coulomb interaction between sites might be less expressed, even in the unperturbed regions, leading to a vanishing of the anomaly in the phonon spectrum.

Between 0.3 and 0.7 mol % of defects, a stronger $4k_F$ anomaly appears due to irradiation, but with clearly different temperature dependence. Here the intensity of the $4k_F$ scattering remains constant from 10 K to room temperature (Fig. 9). Furthermore, width of the $4k_F$ anomaly at these higher doses is also temperature independent. The $4k_F$ scattering appears now as quasielastic, contrasting with its low-concentration behavior. It is more probably due to the perturbed volumes around the strong defects than to be unperturbed matrix, the two-particle Coulomb-interaction term V_{ij} being modulated statistically within this pinned charge-density-wave volume.

We recall, finally, that such a static, i.e., almost temperature independent, $4k_F$ scattering has also been observed in one-dimensional conductors such as quinolium$(TCNQ)_2$ (Ref. 15) and $NMP_{0.59}Phen_{0.41}TCNQ$ [N-methylphenazinium$)_{0.59}$(phenazinium$)_{0.41}$(tetracyanoquinodimethane)].[25]

V. CONCLUSION

One of the main results of the present study is the demonstration that $2k_F$ and $4k_F$ diffuse scattering can still be present in the whole temperature range even when the phase transitions resulting from their condensation into superstructure have completely disappeared and the transport properties have changed so markedly. It is striking to note that there is a large resemblance of x-ray patterns of strongly irradiated TMTSF-DMTCNQ to the patterns of the so-called "pure" $Qn(TCNQ)_2$ or to similar patterns of $NMP_{0.59}Phen_{0.41}TCNQ$ (Ref. 25). In these three cases the following features have been observed: a temperature-dependent $2k_F$ scattering which always keeps the one-dimensional character until 20 K at most, which never condensates in superlattice spots, and which coexists with a $4k_F$ scattering which is almost temperature independent in width and intensity.

ACKNOWLEDGMENTS

The authors acknowledge several fruitful discussions with S. Bouffard, V. J. Emery, S. Kagoshima, C. Noguera, M. Schott, and H. J. Schulz.

*On leave from H. C. Oërsted Institute, Universitetsparken 5, DK-2100 Copenhagen, Denmark.

[1]P. Monceau, N. P. Ong, A. M. Portis, A. Merchaut, and J. Rouxel, Phys. Rev. Lett. 37, 602 (1976).

[2]H. Mutka, L. Zuppiroli, P. Molinie, and J. C. Bourgoin, Phys. Rev. B 23, 5030 (1980).

[3]S. Bouffard, R. Chipaux, D. Jerome, and K. Bechgaard, Solid State Commun. 37, 405 (1980).

[4]J. Gunning and A. J. Heeger, Phys. Status Solidi B 95, 433 (1979).

[5]L. Zuppiroli, H. Mutka, and S. Bouffard, in Proceedings of the International Conference on Low Dimensional Conductors, Boulder, 1981 [Mol. Cryst. Liq. Crystl. 85, 1 (1982)].

[6]L. Zuppiroli, Radiat. Eff. 63, 53 (1982).

[7]G. Mihàly, and L. Zuppiroli, Philos. Mag. A 45, 549 (1982).

[8]C. S. Jacobsen, K. Moretensen, J. R. Andersen, and H. Bechgaard, Phys. Rev. B 18, 905 (1978).

[9]J. P. Pouget, R. Comes, and K. Bechgaard, in *The Physics and Chemistry of Low Dimensional Solids,* edited by L. Alcacer and Nato Asi (Reidel, Dordrecht, 1980), Vol. C56, p. 223.

[10]A. Andrieux, P. M. Chaikin, C. Duroure, D. Jerome, C. Weyl, K. Bechgaard, and J. R. Andersen, J. Phys. Lett. 40, 1199 (1979).

[11]S. Bouffard, M. Ribault, D. Jerome, and K. Bechgaard, J. Phys. C 15, 2951 (1982).

[12]L. Zuppiroli, S. Bouffard, B. Hilti, C. W. Mayer, and K. Bechgaard, Phys. Rev. B 22, 6035 (1980).

[13]L. Forro, A. Janossy, and L. Zuppiroli, J. Phys. (Paris) 43, 977 1982).

[14]L. Zuppiroli, and S. Bouffard, J. Phys. (Paris) 41, 291 (1980).

[15]J. P. Pouget, in Proceedings of the International Conference on Low Dimensional Synthetic Metals [Chem. Scr. 17, 85 (1981)].

[16]J. P. Pouget, P. A. Albony, R. Comes, and K. Bech-

gaard (unpublished).
[17]J. Kondo, and J. Yamaji, J. Phys. Soc. Jpn. B 43, 424 (1977); J. Hubbard, Phys. Rev. 17, 494 (1978); J. Torrance, *ibid.* 17, 3099 (1978).
[18]V. J. Emery, Phys. Rev. Lett. 37, 207 (1976).
[19]H. Mutka, N. Housseau, L. Zuppiroli, and J. Pelissier, Philos. Mag. B 45, 361 (1982).
[20]S. K. Khanna, J. P. Pouget, R. Comes, A. F. Garito, and A. J. Heeger, Phys. Rev. B 16, 1468 (1977).
[21]L. Zuppiroli, P. Delhaes, and J. Amiell, J. Phys. (Paris) 43, 1233 (1982).
[22]P. Trouilloud, S. Bouffard, J. Ardonceau, and L. Zuppiroli, Philos. Mag. B 45, 277 (1982).
[23]G. Milhaly, S. Bouffard, L. Zuppiroli, and K. Bechgaard, J. Phys. (Paris) 43, 1495 (1980).
[24]A. Guinier, *Théorie et Technique de la Radiocristallographie* (Dunod, Paris, 1964), p. 462.
[25]A. J. Epstein, J. S. Miller, J. P. Pouget, and R. Comes, Phys. Rev. Lett. 47, 741 (1981); J. P. Pouget, R. Comes, A. J. Epstein, and J. S. Miller, Mol. Cryst. Liq. Cryst. 85, 1593 (1982).

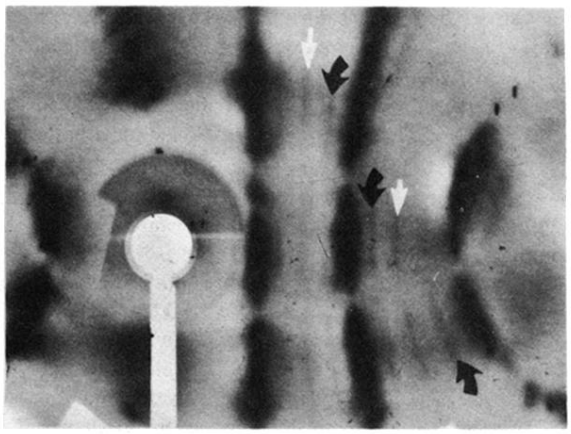

FIG. 1. X-ray pattern of pure TMTSF-DMTCNQ at 125 K showing the $2k_F$ (black arrows) and $4k_F$ (white arrows) diffuse lines, at $0.25a^*$ and $0.50a^*$ reduced-zone wave vectors, respectively, coming from the intersection of the Edwald sphere with diffuse sheets at the corresponding wave vector. In this pattern the a chain direction is horizontal and the reciprocal space shown is close to the (a^*,b^*) plane. (This pattern, from Ref. 15, is free from $\lambda/2$ contamination.)

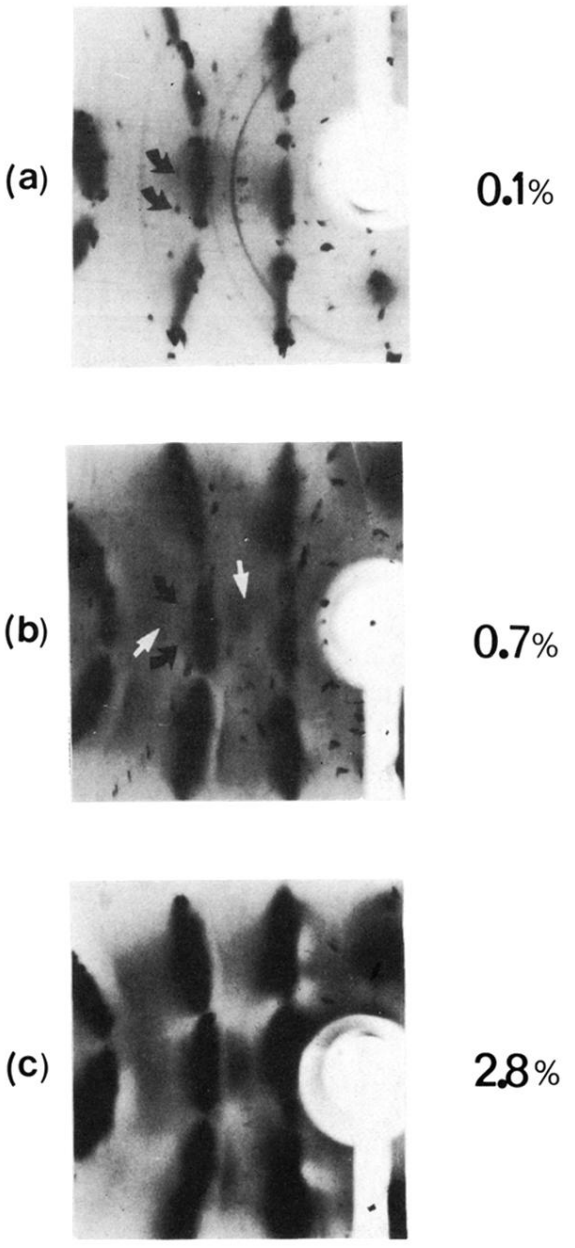

FIG. 2. X-ray patterns of TMTSF-DMTCNQ at 10 K, for various defect concentrations. They have been taken nearly in the same orientation as in Fig. 1. (a) 0.1 mol % of defects; black arrows point to the $2k_F$ scattering condensed into well-defined satellite reflections at $\vec{q}=(\frac{1}{4},\frac{1}{3},0)$ reduced wave vector. No $4k_F$ scattering can be detected (additional Bragg spots in layers $h=0.5a^*$ and $1.5a^*$ are due to $\lambda/2$ contamination and rings observed around the incident beam is diffraction coming from the sample holder). (b) 0.7 mol % of defects: black arrows point to the previous satellite reflections noticeably broadened along b^*. Weak diffuse lines are also present at the $4k_F$ wave vector (white arrows). (c) 2.8 mol % of defects: only $2k_F$ lines are clearly visible (the modulation of their intensity in line direction comes mostly from x-ray interferences between Se atoms of the TMTSF molecule). These $2k_F$ lines are asymetrically broadened along a^* toward the position of the $4k_F$ anomaly which is now undetectable by eye. It is worth mentioning at such a low temperature, the large increase of the diffuse intensity surrounding main Bragg reflections when one passes from x-ray patterns (a) to (c). This reflects, via the x-ray scattering, the increasing amount of disorder on the average lattice, induced by the increasing number of defects created by irradiation.